IJE TRANSACTIONS B: Applications Vol. 37 No. 02, (February 2024) 268-282

International Journal of Engineering

Journal Homepage: www.ije.ir

Seismic Fragility of FRC Columns using Incremental Dynamic Analysis and eXtended Finite Element Method

S. El Yassari*, A. EL Ghoulbzouri, S. El Janous

MODSGC Unit, National School of Applied Sciences Al Hoceima, University Abdelmalek Essaadi, Tangier, Morocco

P A P E R I N F O

Paper history:
Received 24 July 2023
Received in revised form 26 September 2023
Accepted 27 September2023

Keywords:
Fiber Reinforced Concrete
Incremental Dynamic Analysis
Pushover Analysis
Concrete Damage Plasticity
XFEM
Extended Finite Element Method

A B S T R A C T

Ensuring seismic resilience in earthquake-prone regions is imperative for structural safety. Fiber-Reinforced Concrete (FRC) columns hold promise for enhancing structural performance under seismic conditions. This study seeks to comprehensively evaluate their seismic behavior. The primary objective of this research is to assess and compare the seismic performance of various FRC column types, including polypropylene fibers (PFRC), steel fibers (SFRC), and hybrid combinations (HyFRC), in contrast to conventional reinforced concrete (RC) columns. To achieve this, the study employs eXtended Finite Element Method combined with Concrete Damage Plasticity (XFEM-CDP) in Abaqus to scrutinize static and dynamic responses. The nonlinear static pushover analysis unveiled a notable improvement in seismic resistance across all FRC types when compared to RC columns. Incremental dynamic analyses (IDA) are conducted using the selected suite of 10 near fault as-recorded ground motions to evaluate the inelastic seismic responses of different FRC bridge columns. XFEM-CDP simulations in Abaqus captured multiple aspects of FRC columns, such as concrete cracking, loss of stiffness and plastic behavior. Seismic fragility analysis of these FRC columns is conducted considering four damage states: a) longitudinal steel yielding, b) core concrete crushing, c) steel bar buckling, and d) longitudinal steel bar fracture. The results indicated that HyFRC columns exhibit the lowest damage vulnerability compared to PFRC and SFRC variants.

***doi**: 10.5829/ije.2024.37.02b.05*

Graphical Abstract

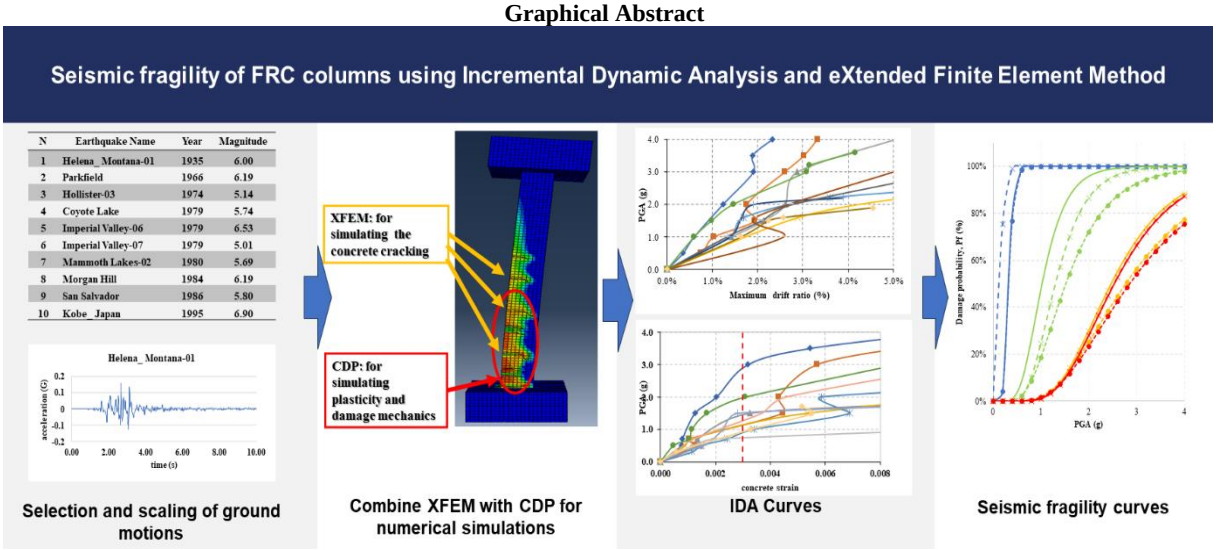

[1] Corresponding author email: *soufiane.elyassari1@etu.uae.ac.ma* (S. El Yassari)

Please cite this article as: El Yassari S, EL Ghoulbzouri A, El Janous S. Seismic Fragility of FRC Columns using Incremental Dynamic Analysis and eXtended Finite Element Method. International Journal of Engineering, Transactions B: Applications. 2024;37(02):268-82.

1. INTRODUCTION

Reinforced Concrete (RC) bridges are extensively built across the globe, with a significant portion of them situated in regions prone to seismic activity. In compliance with contemporary seismic regulations, these structures are mandated to maintain adequate capacity to endure a catastrophic earthquake. Nonetheless, recent substantial seismic events, such as the 2011 Japan earthquake (Mw 9.0) and the 2023 Turkey earthquake (Mw 7.8), resulted in extensive damage. This damage can be attributed, in part, to the inherent limitations of plain concrete, which includes a lack of flexural strength, brittleness, low toughness, and limited energy absorption capabilities.

Traditionally, increasing transverse stirrups in bridge columns enhances concrete properties. However, this can lead to construction problems. An alternative solution gaining traction is fiber-reinforced concrete (FRC). FRC integrates various fiber types like steel and polypropylene, improving tensile strength, toughness, and flexural strength. It also enhances ductility and energy absorption during seismic events.

Various studies investigate FRC in bridge columns, including steel fiber (SFRC), polypropylene fiber (PFRC), and hybrid fiber (HyFRC) types. SFRC enhances ductility and loading capacity, with an optimal volume fraction of 1.5% for shear strength (1). PFRC boosts ductility and energy absorption. HyFRC shows superior dynamic capacity, especially at higher axial compression ratios.

Existing research on FRC columns lacks a holistic evaluation under diverse seismic scenarios and materials. Additionally, the comparative advantages of different fiber types for seismic resilience have not been fully explored. Seismic analyses have conventionally relied on linear and simplified static or dynamic methods, which may not fully represent the intricate interactions between seismic forces and structural behavior in reality. Probabilistic approaches, such as the development of fragility curves, have emerged as a promising alternative for seismic assessments (2-5).

Over the past two decades, the field of structural seismic assessment has rapidly advanced with the probabilistic approach. Fragility curves, which estimate the interdependence between structural demands and capacity, have become standard in seismic assessments (3). Various methodologies have been proposed for generating structural seismic fragility curves, encompassing empirical and analytical approaches (3-8). Analytical methods, including elastic-spectral (3-5), non-linear static (7-10), and non-linear dynamic analyses (11-15), have emerged as diverse and numerous fragility generation methodologies.

The performance-based earthquake engineering (PBEE) procedure necessitates evaluating the interplay between structural capacity and seismic demands. To address this, the Incremental Dynamic Analysis (IDA) was introduced by Luco and Cornell (16), further developed by Vamvatsikos and Cornell (17), enabling the prediction of a structure's response ranging from elastic behavior to inelastic behavior and ultimately collapse.

Non-linear methods, such as Nonlinear Static Pushover Analysis (NSPA) and IDA, are widely employed due to their relative accuracy in structural design and seismic analysis. Pushover analysis, a non-linear static method, offers a quick evaluation of a structure's seismic performance (18, 19). In contrast, IDA, incorporating dynamic effects into nonlinearity, provides more accurate results than non-linear static analysis. Although non-linear dynamic methods require more computational time and effort, advancements in computing power have increased their popularity in recent years.

Traditional methods of seismic analysis have often proven inadequate in capturing the complex nonlinear behavior of structures subjected to strong earthquakes. To address this limitation and improve the accuracy of seismic assessments, researchers have been pioneering an innovative approach by combining Computational Damage Plasticity (CDP) and the eXtended Finite Element Method (XFEM) within the Abaqus software framework. This synergistic integration allows for a comprehensive evaluation of structural response under seismic loading conditions, incorporating both NSPA and IDA.

This paper aims to assess of the seismic performance of FRC columns. 3D nonlinear finite element models have been constructed within the Abaqus software to simulate the seismic behavior of these FRC columns.

These models are first calibrated using available experimental data from the literature. The seismic

TABLE 1. Summary of the material properties

Material	Diameter (mm)	Length (mm)	Density (g/cm^3)	Tensile /compressive strength (MPa)	Elastic modulus (GPa)
Concrete	-	-	2.5	40	30
Longitudinal steel	20	-	7.85	400	200
Hoop steel	12	-	7.85	335	200
Steel fibers	0.55	35	7.85	1143	200
Polypropylene fibers	0.048	19	1.2	400	43

resilience of columns employing various FRC materials is evaluated by considering four flexural damage states: longitudinal reinforcement yielding, concrete crushing, buckling of reinforcement, and longitudinal reinforcement fracture. These damage states are derived through NSPA.

Furthermore, IDA is conducted to examine the seismic demands placed on FRC columns subjected to intense ground motions. In the IDA approach, a selection of ten near-fault ground motions is employed as seismic inputs for the finite element models. These ground motions are scaled to different intensity levels. The outcomes of IDA are presented in the form of IDA curves, illustrating the relationship between the engineering demand parameter (EDP) of the structures and the intensity measure (IM) of the ground motions. For this study, peak ground acceleration (PGA) is adopted as the IM. Various EDPs of the bridge columns, such as maximum drift, longitudinal steel strain, and concrete strain demands, were identified and documented throughout the IDA analysis. finally, the seismic fragility curves were constructed and compared to explore the impact of different FRC materials on the seismic performance of the columns.

2. MODELING OF DIFFERENT FRC COLUMNS

2. 1. Details of Columns Figure 1 provides the dimensions of the studied column, which consists of 20 longitudinal reinforcement bars with a diameter of 20 mm, resulting in a steel-to-concrete ratio of 2%. The column has a height of 6 meters and a square cross-section measuring 0.6 m by 0.6 m. The pile cap dimensions are 1.8 m by 1.8 m by 0.8 m, while the foundation measures 1.8 m by 1.8 m by 0.8 m. The square transverse stirrups have a diameter of 12 mm and are spaced at intervals of 150 mm.

This study focuses on four different types of columns: RC (conventional reinforced concrete), SFRC (steel fiber-reinforced concrete), PFRC (polypropylene fiber-reinforced concrete), and HyFRC (a hybrid combination of steel and polypropylene fibers). The material characteristics for each type are presented in Table 1. The parameters for the steel fibers were adopted from literature (20), while those for the polypropylene fibers were derived from literature (21). The steel fibers have a tensile strength of 1143 MPa, an elastic modulus of 200 GPa, and a density of 7.8 g/cm³.

To ensure the workability of the concrete mixture is not compromised, the recommended optimal volume fraction of steel fibers in the SFRC columns is 1.5% (117 kg/m³). The PFRC columns contain a volume fraction of 0.15% (1.37 kg/m³) of polypropylene fibers. Previous research by Huang et al. (21), Yin et al. (22) suggested that the optimal fiber combination for enhancing concrete strength in the HyFRC is 1.5% steel fibers and 0.15% polypropylene fibers. Table 2 provides the main parameters for the various FRC columns.

2. 2. Finite Element Modeling Finite element models of columns made of standard RC and FRC materials are created using the commercial software Abaqus. Truss elements are used to simulate the rebars, and solid three-dimensional eight-node linear brick with full integration (C3D8) simulates the concrete elements. The dynamic implicit algorithm Newton method with transient fidelity is used to implement the time-history analysis. The concrete damaged plasticity model (CDP) (23, 24) has been used to describe the stiffness degradation of concrete during cyclic loading, which can be defined using two factors, dt and dc (Figure 2). The compressive and tensile damage factors, dc and dt are estimated based on the corresponding inelastic strains using Equations 17-22 (25).

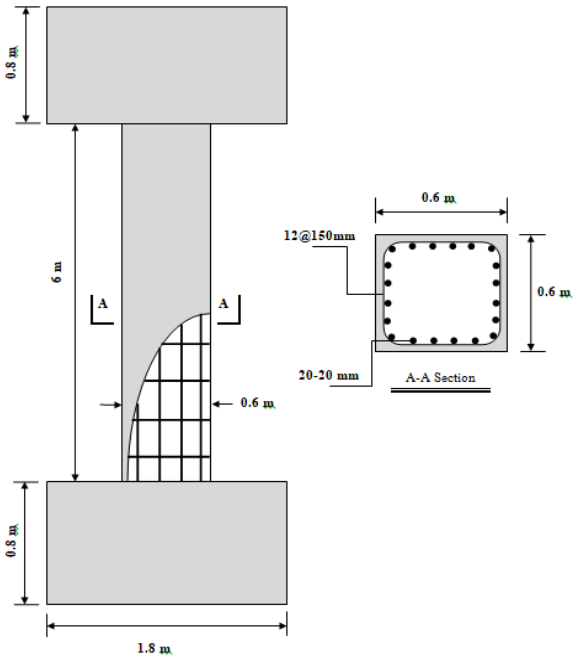

Figure 1. Column dimensions and reinforcement details

TABLE 2. Main parameters for different bridge columns

Material	Compressive strength (MPa)	Steel fiber content	Polypropylene fiber content
RC	40	-	-
SFRC	45	1.50%	-
PFRC	43	-	0.15%
HyFRC	48	1.50%	0.15%

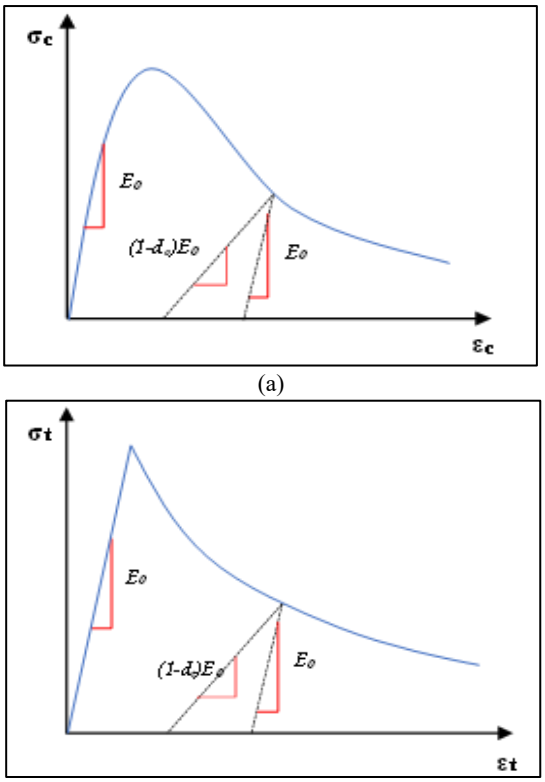

Figure 2. Stress-strain relationships of CDP in ABAQUS, (a) compressive curve, (b) tensile curve

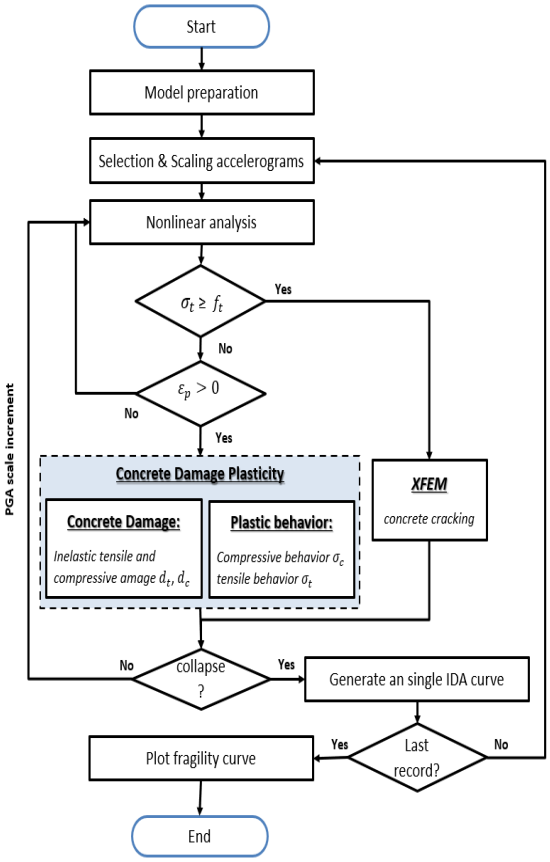

Figure 3. Flowchart of combined XFEM/CDP method

The ABAQUS software simulates crack propagation using the eXtended Finite Element Method (XFEM), while material nonlinearities are accounted for using CDP criteria. XFEM is used in the simulation to solve the discontinuity problems.

In practice, discontinuities can manifest as flaws or cracks. There are various kinds of discontinuity:

- A strong discontinuity represents the cracks.
- A weak discontinuity represents the interface between two different materials.

It is challenging to analyze the discontinuity in a concrete model using the traditional finite element method. Without the need for remeshing, XFEM can simulate the initiation and propagation of a discrete crack along any solution path. The combination of XFEM and CDP in this paper is presented in Figure 3.

2. 3. Material Property

2. 3. 1. Compressive Behavior The compressive behavior model in this study is based on Abadel et al.'s (26) work:

$$\sigma_c = \left(\frac{\beta\left(\frac{\varepsilon_c}{\varepsilon_0}\right)}{\beta-1+\left(\frac{\varepsilon_c}{\varepsilon_0}\right)^{\beta}}\right) f_{cu} \quad (1)$$

where f_{cu}denotes the ultimate compressive stress, ε_c and ε_0 represents the compressive strain and the strain at peak stress of plain concrete (= 0,002), respectivly.

The parameters can be calculated using the following equations:

$$\beta = 1 + 5e^{-1,376RI_v} \quad (2)$$

$$\beta_0 = 0,108f_c - 0,966 \quad (3)$$

$$f_{cfrc} = f_{c0} + 5,222RI_v \quad (4)$$

$$\varepsilon_{frc} = \varepsilon_{c0} + 0,0004RI_v \quad (5)$$

$$RI_v = \sum RI_{vi} \quad (6)$$

$$RI_{vi} = V_i \frac{l_i}{d_i}\frac{E_i}{E_s} \quad (7)$$

For the plain concrete, the value of parameter $\beta_0$can be calculated with the help of Equation 3. RI_v, V_i,l_i, and d_i denote thereinforcing index, fibers' volume fraction, length, and diameter (or their corresponding diameter in non-circular sections), E_i and E_s are the fiber's and steel material's modulus of elasticity, respectively.

2. 3. 2. Tensile Behavior The tensile stress-crack opening displacement relationship adopted for plain concrete in this paper has been proposed by Hordijk (27). whereas for HFRC, the constitutive relationship was developed by Almusallam et al. (28) which is based on the reinforcing index, RIv:

$$\frac{\sigma_t}{f_t} = \left(1 + \left(c_1 \frac{w_t}{w_{cr}}\right)^3\right) e^{\left(-c_1 \frac{w_t}{w_{cr}}\right)} - \frac{w_t}{w_{cr}}(1 + c_1{}^3) e^{(-c_1)} \quad (8)$$

$$f_t = 1{,}4\left(\frac{f_{cu}-8}{10}\right)^{2/3} \quad (9)$$

$$G_F = \left(0{,}0469 d_a{}^2 - 0{,}5 d_a + 26\right)\left(\frac{f_{cu}}{10}\right)^{0{,}7} \quad (10)$$

$$w_{cr} = 5{,}14 \frac{G_F}{f_t} \quad (11)$$

In these equations, the f_t is the tensile strengths of plain concrete, w_t, w_{cr} denotes the crack opening displacement and crack displacement at the complete loss of tensile stress, respectivly. d_a and l_{eq} represent the maximum aggregate size of the concrete (20 mm) and the mesh element length, respectivly.

Concerning the tensile behavior of FRC, $\sigma_t(w)$, Rousakis et al. (29) proposed an analytical model to describe the tensile softening behavior based on the reinforcing index, RIv. This model was obtained through inverse analysis and provides a good agreement with experimental results.

$$\sigma_t(w_t) = a_1 f_{tfrc} e^{(-a_2 w_t)} \quad (12)$$

$$a_1 = 0{,}75 \quad (13)$$

$$a_2 = 10 e^{-4{,}3 RI_v} \quad (14)$$

$$f_{tfrc} = (f_t - 1) + e^{1{,}23 RI_v} \quad (15)$$

where f_{tfrc} denotes the tensile strength of FRC.

It was assumed that each element has a single crack. thus, the relationship between strain and the crack opening displacement is defined by Equation 14.

$$\varepsilon_t = \varepsilon_{tm} + w_t / l_{eq} \quad (16)$$

ε_{tm} is the tensile strain corresponding to the tensile strengths.

2. 3. 3. Concrete Damage Plasticity Model The compressive and tensile damage factors, dc and dt are given by Equations 15-20.

$$d_t = \frac{1}{e^{-\frac{1}{m_t}} - 1}\left(e^{-\frac{\varepsilon_{t,nom}^{ck}}{m_t}} - 1\right) \quad (17)$$

$$d_c = \frac{1}{e^{-\frac{1}{m_c}} - 1}\left(e^{-\frac{\varepsilon_{c,nom}^{in}}{m_c}} - 1\right) \quad (18)$$

$$\varepsilon_{t,nom}^{ck} = \frac{\varepsilon_t^{ck}}{\varepsilon_{tu}^{ck}} \quad (19)$$

$$\varepsilon_{c,nom}^{in} = \frac{\varepsilon_c^{in}}{\varepsilon_{cu}^{in}} \quad (20)$$

m_c,m_t, are the parameters that control damage evolution speed. $\varepsilon_{t,nom}^{ck}$, $\varepsilon_{c,nom}^{in}$denote the normalized compressive and tensile inelastic strains.ε_{tu}^{ck},ε_{cu}^{in}, are the corresponding ultimate strains.

Typically, for plain concrete, Chi et al. (25) suggested the use of $m_t = 0{,}05$, $m_c = 0{,}1$, $\varepsilon_{cu}^{in} = 0{,}033$, $\varepsilon_{tu}^{ck} = 0{,}0033$.

For FRC, parameters m_c^{hf} and m_t^{hf} are modified according to the composite material theory as follows:

$$m_c^{hf} = m_c\left(1 + a_{m1}\lambda_{sf} + b_{m1}\lambda_{pf}\right) \quad (21)$$

$$m_t^{hf} = m_t\left(1 + a_{m2}\lambda_{sf} + b_{m2}\lambda_{pf}\right) \quad (22)$$

where λ_{sf} and λ_{pf} are the characteristic parameters of steel and polypropylene fibers, respectively.

The values am1 = 0.452, bm1 = 0.054, am2 = 0.628, and bm2 = 0.156 were recommended by Chi et al. (25).

The key parameters, K_c^{hf}, $\sigma_{b0}^{hf}/\sigma_{c0}^{hf}$ and the dilation angle ψ^{hf} are defined based on the following equations:

$$K_c^{hf} = K_c . \frac{k_t}{k_c} \quad (23)$$

$$k_t = 1 + 0{,}080\lambda_{sf} + 0{,}132\lambda_{pf} \quad (24)$$

$$k_c = 1 + 0{,}056\lambda_{sf} \quad (25)$$

$$\lambda_{sf} = V_{sf} \frac{l_{sf}}{d_{sf}} \quad (26)$$

$$\lambda_{pf} = V_{pf} \frac{l_{pf}}{d_{pf}} \quad (27)$$

$$\frac{\sigma_{b0}^{hf}}{\sigma_{c0}^{hf}} = \frac{k_t{}^2}{0{,}132 k_c}\left[\left(0{,}728 - \frac{0{,}749}{k_t}\right) + \sqrt{\left(0{,}728 - \frac{0{,}749}{k_t}\right)^2 + \frac{0{,}03}{k_t{}^2}}\right] \quad (28)$$

$$\psi^{hf} = \psi_0(1 - a_\psi \lambda_{sf} - b_\psi \lambda_{pf}) \quad (29)$$

$$\psi^{hf} = \psi_0(1 - a_\psi \lambda_{sf} - b_\psi \lambda_{pf}) \quad (30)$$

$$\psi_0 = 36 + (\sigma_{c0}/\sigma_{cm0}) \quad (31)$$

In this equation, σ_{c0} is a parameter that ensures the equivalence of units, and σ_{cm0} is recommended to be 10 MPa according to (29). The coefficients $a_\psi$and b_ψ, which are obtained from (25), have values of 0.861 and 0.097, respectively. These coefficients are used to calculate the dilation angle for plain concrete in the proposed model.

2. 3. 4. Concrete Crack Evolution Law In standard FEM, cracks must follow element edges or a

predefined path, such as the cohesive zone model. In contrast, the XFEM does not need the crack path to be predefined, making it independent of the model mesh. In the XFEM, Crack initiation criteria must be specified. This study uses the ultimate tensile strength ft as the crack initiation criteria. On the other hand, crack evolution is determined based on the displacement parameter and Equations 8 and 12, as shown in Figure 4. The XFEM can be implemented in Abaqus Implicit to simulate the concrete cracking process using the parameters listed in Table 3.

2. 3. 5. Steel Material Model The reinforcing steel bars in the concrete columns were modeled as truss elements (T3D2) with linear elastic behavior, followed by linear hardening until reaching the ultimate stress in tension (σu). The strain-softening and the fracture of the bars are simulated in Abaqus using the damage fracture option, where (wf) is the estimated displacement at failure based on calibration with test results (Figure 5). For simplification purposes, the bond between concrete and steel is assumed to be perfect. The debonding of steel is simulated as steel degradation. Table 4 shows the mechanical properties used in the reinforcing steel material model.

2. 3. 6. Model Validation with Experimental Results from the Literature Quasi-static cyclic pushover analyses were performed using the Abaqus software to simulate the behavior of the columns. Finite element models of columns incorporating different RC and FRC materials were calibrated and validated using experimental data from previous studies (20, 21, 30). The main parameters for the various FRC columns are summarized in Table 5.

Constitutive models for the steel bars and concrete matrix components were separately established for numerical modeling. Truss elements (T3D2) were used to model the stirrups, while a solid three-dimensional eight-node linear brick with full integration (C3D8) was assigned to represent the concrete matrix. It is worth noting that full integration elements (C3D8) were utilized as they converge faster with the eXtended Finite Element Method (XFEM) compared to reduced integration elements (C3D8R).

Figure 6 illustrates the hysteretic curves and corresponding skeleton curves of the ten different types of RC, SFRC, PFRC, and HyFRC columns. The solid black line represents the experimental results, while the dashed red line represents the numerical simulation results. The figure demonstrates the cyclic deterioration of these columns' performance, including the gradual decrease in unloading stiffness, the degraded strength resulting from cyclic loading, and the pinching effect caused by concrete cracking.

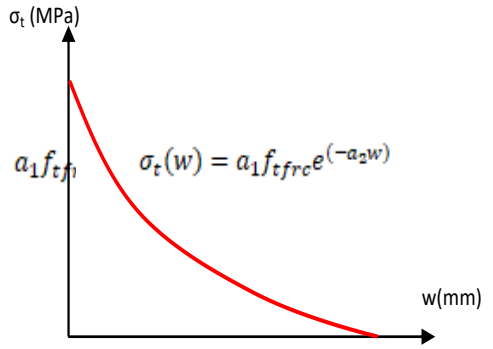

Figure 4. Tensile strength and Crack evolution relationship for FRC

TABLE 3. XFEM parameters

	RC	FRC
Crack initiation	ft	a1*ftFRC
Crack evolution law	Exponential	Exponential
evolution law parameter	c1/wcr	a2
Displacement at failure	wcr	2/a2

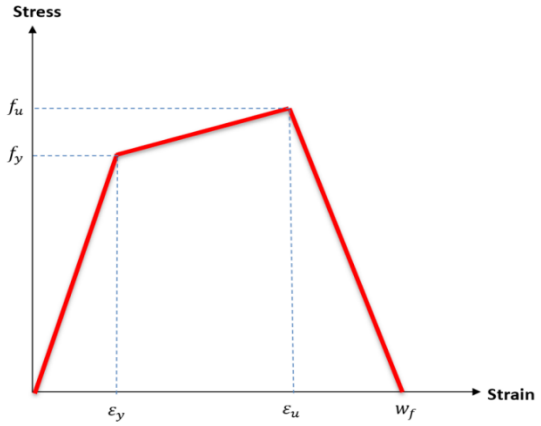

Figure 5. Reinforcing steel model for steel bars

TABLE 4. Steel parameters for different models

Model	d (mm)	fy (MPa)	fu (MPa)	Es (MPa)	εh	εu
(a). Zhang2013	10	335	500	2.0*105	0.001675	0.06
(b). Zhang2017	14	335	500	2.0*105	0.001675	0.06
(c). Huang2015	14	553.9	670.3	2.0*105	0.001675	0.06
(d). Liang2016	16	440	609	1.95*105	0.001675	0.08

TABLE 5. Values for CPDM for (a, b, c, d) normal RC, (e, f, g) SFRC, (h) PFRC and (i) HYFRC

Model	Vsf (%)	Vpf (%)	ψ (°)	$\sigma_{b0}^{hf}/\sigma_{c0}^{hf}$	K	Mesh size (mm)
(a). RC-Zhang2017	0.0	0.0	38.70	1.162	0.666	50
(b). RC-Liang2016	0.0	0.0	38.70	1.162	0.666	60
(c). SFRC-Zhang2017	1.0	0.0	16.775	1.46	0.676	50
(d). PF-1-1-Huang2015	0.0	0.15	34.968	1.162	0.718	40
(e)-(f). HF-1-1-Huang2015	1.5	0.15	4.085	1.641	0.731	40

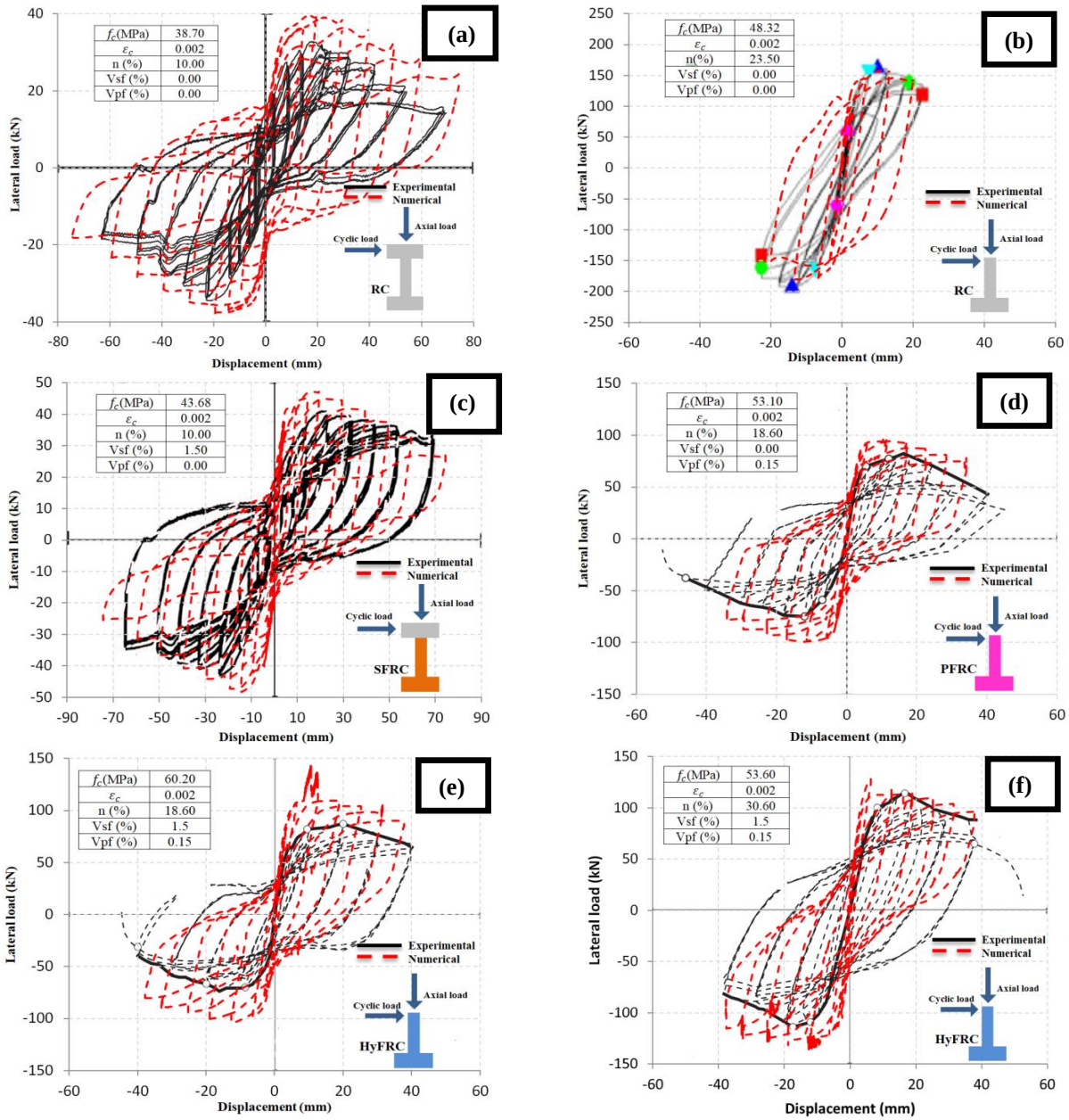

Figure 6. Comparison of the numerical hysteresis curve of different columns with the experimental hysteresis response: a, b) RC (12, 21), c) SFRC (12), d) PFRC (13) and e, f) HyFRC (13)

The comparison results are shown in Figure 6 indicate that the dynamic hysteretic model can provide reasonable estimates of the strength capacity of the various FRC columns. Furthermore, the proposed degradation parameters accurately depict the deterioration of strength and stiffness, as well as the pinching effect observed in the experimental data.

The analytical model introduced by Zhang and Dias-da-Costa (20), exhibited the most significant difference between the predicted load and the actual test results. This discrepancy can be primarily attributed to the utilization of a relatively large mesh size, as indicated in Table 5 (50 mm). Notably, larger mesh elements necessitate higher fracture energies, leading to more substantial inaccuracies in lateral load predictions. This highlights the significance of conducting a sensitivity analysis concerning mesh size, particularly since more pronounced errors tend to manifest at smaller displacements.

2. 4. Nonlinear Static Pushover Analysis

The finite element model included the weight load of the materials, with concrete density of 2500 kg/m^3 and steel density of 7850 kg/m^3. The superstructure load of 171 kN and lateral load were applied at the top of the pile cap. Consequently, the columns had an axial load ratio determined as 0.02 times the product of concrete strength (fc) and column section area (Ac). The results of the nonlinear static pushover analysis (NSPA) established the relationship between the shear base and lateral displacement, commonly known as pushover curves. The deformed shape and the tensile damage of different RC and FRC columns are presented in Figure 7.

Figure 8 illustrates the pushover curves of the different reinforced concrete (RC) and fiber-reinforced concrete (FRC) columns. As depicted, all FRC columns exhibited significantly increased capacity compared to the standard RC column. Among the FRC columns, the HyFRC column demonstrated the most substantial enhancement in seismic capacity, followed by the SFRC and PFRC columns. Moreover, the variations in pushover curves between the SFRC, PFRC, and HyFRC columns were minimal at small lateral displacements, primarily due to the similar elastic modulus of these FRC materials.

The differences between the SFRC and PFRC columns became less significant at larger lateral displacements, as the improvement in compressive strength offered by both types of fibers was comparable. Overall, all FRC materials exhibited a significant improvement in seismic capacity.

The structural damage classification according to HAZUS includes "Slight, Moderate, Extensive, and Collapse." This paper considers four flexural damage states: a) longitudinal steel yielding, b) core concrete crushing, c) steel bar buckling, and d) longitudinal steel bar fracture. The limit values for these damage states can be determined based on the strain limits of concrete and steel bars.

It is assumed that longitudinal steel bars yield when the steel strain reaches the ratio of yield stress to elastic modulus of the steel bars. According to Paulay and Priestley (31), core concrete crushing occurs when the concrete strain reaches 0.003, and sometimes higher values such as 0.006 to 0.008 are observed. The ultimate compression strain of 0.004 is recommended. ACI and AASHTO propose a design maximum strain of concrete crushing at 0.003. In this paper, a concrete crushing strain of 0.003 is adopted as the reference value. Furthermore, the buckling and fracture of steel bars can be predicted using the model projected by Berry and Eberhard (32) based on the tensile strain of longitudinal reinforcements.

Table 6 presents the lateral displacements and base shear obtained from the pushover curves at the four flexural damage states.

$$\varepsilon_{bb}^{calc} = 0.045 + 0.25\rho_{eff} \quad (32)$$

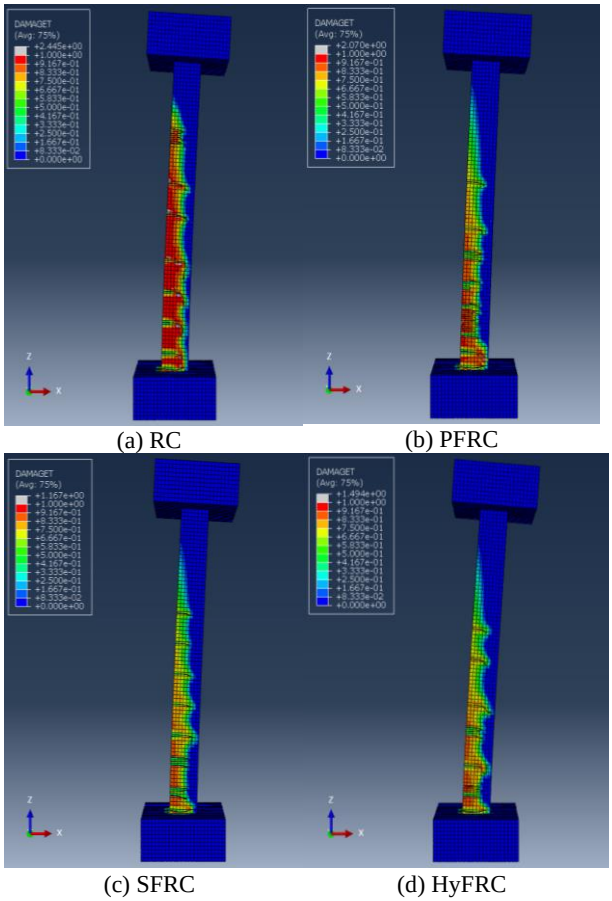

(a) RC (b) PFRC

(c) SFRC (d) HyFRC

Figure 7. Tensile damage results for different column types: a) RC, b) PFRC, c) SFRC and d) HyFRC

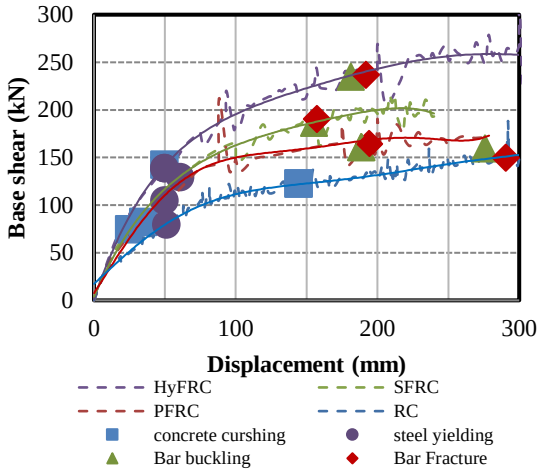

Figure 8. Pushover curves for different FRC columns

$$\varepsilon_{bf}^{calc} = 0.045 + 0.3\rho_{eff} \quad (33)$$

$$\rho_{eff} = \rho_s f_{ys}/f'_c \quad (34)$$

where ρ_{eff} is the effective confinement ratio, $\rho_s$is the spiral-reinforcement ratio, and $f_{ys}$is the yield stress of the spiral reinforcement.

Table 6 reveals that incorporating fibers into concrete enhances the shear base of columns. The slight damage state (longitudinal steel yielding) initiates at the same level of displacement in all columns for the steel yielding limit state. Normal RC columns have a base shear at steel yielding that is 79.25 kN, 31.8%, 62.7%, and 75.1% lower than SFRC, PFRC, and HyFRC columns, respectively. The base shear is enhanced in all columns for the FRC columns at extensive and collapse damage states, such as longitudinal bar buckling and fracture.

TABLE 6. Relative difference of base shear and displacement at different damage states

Material	Steel yielding		Concrete crushing		Steel buckling		Steel fracture	
	Displacement (mm)	Base shear (kN)	Displacement (mm)	Base shear (kN)	Displacement (mm)	Base shear (kN)	Displacement (mm)	Base shear (kN)
RC	51.31	79.25	144.46	122.5	275.95	159.2	290.67	149.5
PFRC	49.97	104.5	34.96	82.15	188.58	160.9	194.21	164
SFRC	60.87	129	25	74.23	155.44	186.2	157.4	190.4
HyFRC	49.74	138.8	49.95	142.1	181.22	234.6	191.84	236.8

3. INCREMENTAL DYNAMIC ANALYSIS

While NSPA can predict potential weak points in the structure under a lateral load, but it cannot be used to determine the dynamic effect of a given seismic excitation. On the other hand, the NTHA can predict the seismic demands with better accuracy. The IDA method is based on the NTHA for estimating significant inelastic responses of structures.

Damage measures such as drift ratio and displacement of the column's top are directly connected with the failure mechanism, which enables them to be considered as Engineering Demand Parameter (EDP) when generating IDA curves. On the other hand, the Peak Ground Acceleration (PGA) is selected as intensity measure (IM).

The IDA method is used in this paper to investigate the damage of columns and determine damage state limits under each ground motion. The steps required by the analysis (17):

1) Choose a set of records of seismic events that are representative of the hazard level;
2) Select a specific records and scale it using a scaling factor;
3) Perform a NTHA of the structure using this scaled record and identify the EDP and the IM of the ground motions;
4) Choose a set of records of seismic events that are representative of the hazard level;
5) Select a specific records and scale it using a scaling factor;
6) Perform a NTHA of the structure using this scaled record and identify the EDP and the IM of the ground motions;
7) Gradually increase IM using the scaling factor of this record until cover so that the simulations can cover the entire response range from the elastic behavior to total collapse;
8) Repeat Steps 2-4 for the same record;
9) Plot these points in order to generate the IDA curve

3. 1. Ground Motions A set of 10 Earthquakes with magnitude ranging from 6.0 to 8.0 are selected from the PEER database and used to evaluate the seismic performance of columns, as summarized in Table 7. These ground motions have wave velocities Vs in the upper 30 m ranging from 200 m/s to 600 m/s. The records' closest site-to-fault distances range from 0.1 to 10 km. Figure 9 depicts the spectral accelerations of the ground motions, which demonstrated they can accurately represent medium to strong earthquakes.

3. 2. Maximum Drift Demand A single Incremental Dynamic Analysis (IDA) curve is generated

TABLE 7. Selected ground motions used in IDA

N	Earthquake Name	Year	Station Name	Magnitude	Rrup (km)	Vs30 (m/sec)
1	Helena_ Montana-01	1935	Carroll College	6.00	2.86	593.35
2	Parkfield	1966	Cholame - Shandon Array #5	6.19	9.58	289.56
3	Hollister-03	1974	San Juan Bautista_ 24 Polk St	5.14	9.11	335.5
4	Coyote Lake	1979	Coyote Lake Dam - Southwest Abutment	5.74	6.13	561.43
5	Imperial Valley-06	1979	Brawley Airport	6.53	10.42	208.71
6	Imperial Valley-07	1979	El Centro Array #5	5.01	11.23	205.63
7	Mammoth Lakes-02	1980	Convict Creek	5.69	9.46	382.12
8	Morgan Hill	1984	Anderson Dam (Downstream)	6.19	3.26	488.77
9	San Salvador	1986	Geotech Investig Center	5.80	6.30	489.34
10	Kobe_ Japan	1995	Kobe University	6.90	0.92	1043

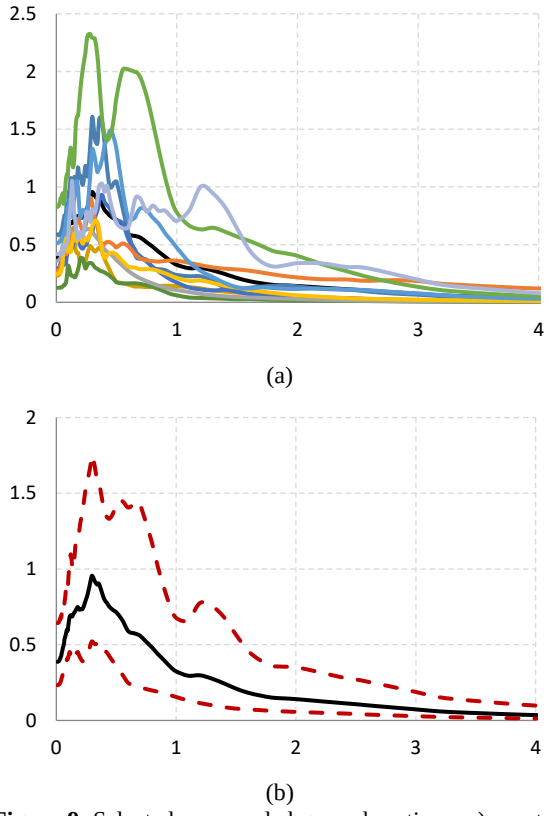

Figure 9. Selected as-recorded ground motions: a) spectral acceleration and b) percentiles of spectral

by measuring the maximum drift ratio of the column under incremental ground motion intensity levels. Figures 10-13 illustrates the IDA curves for SFRC, PFRC, and HyFRC columns, indicating both linear and nonlinear components that capture the elastic and inelastic behavior of structures subjected to varying Peak Ground Acceleration (PGA) intensities. The IDA curves effectively describe the softening behavior of the columns in the inelastic range until collapse occurs.

Due to the uncertainty of ground motions, the IDA curves exhibit diverse and scattered data, necessitating the use of statistical tools for evaluation. To provide more objective and reliable data, the IDA curves are analyzed using the 20th, 50th, and 80th fractile values. Figure 11

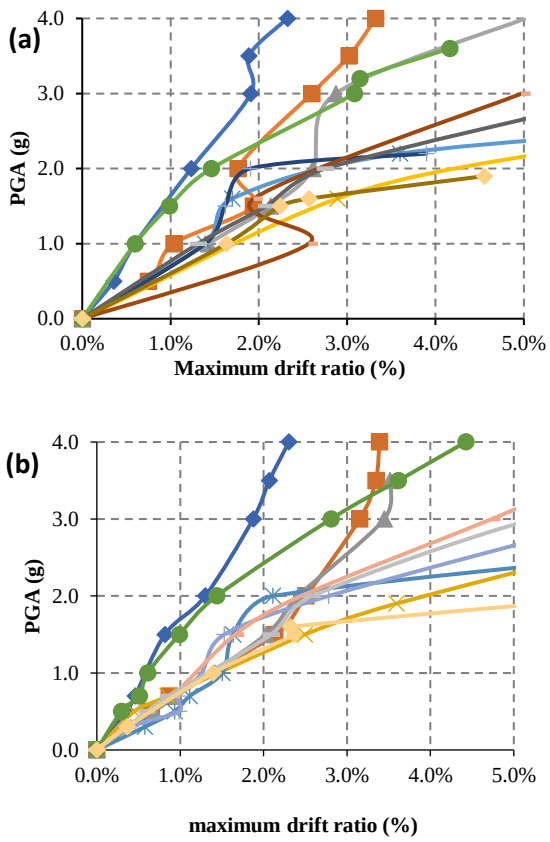

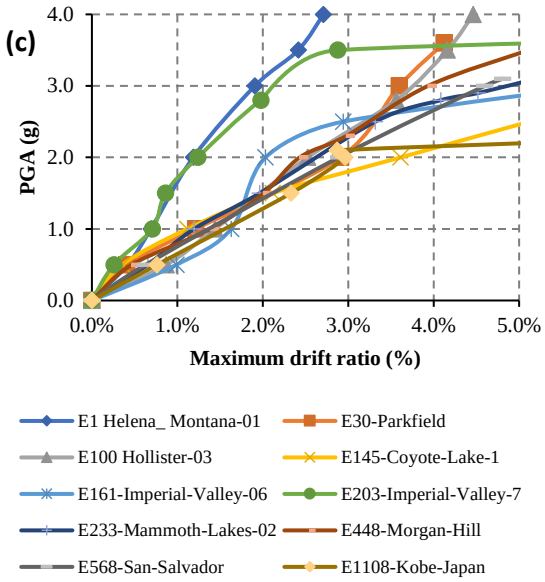

Figure 10. IDA curves for maximum drift (%) of different FRC columns: a) PFRC; b) SFRC and c) HyFRC

presents the median and percentiles of the maximum drift IDA curves for columns made of standard Reinforced Concrete (RC) and various Fiber-Reinforced Concrete (FRC) materials. It should be noted that for larger PGA values, the remaining number of IDA curves becomes small, making statistical calculation unrealistic. Therefore, the PGA range used for the fractile IDA curves is smaller than that of the original IDA curves.

From the results, it can be concluded that PFRC, SFRC, and HyFRC are all effective in improving seismic capacity and reducing seismic demands on columns. The improvement in seismic performance among the different FRC materials is negligible, with only a 5% difference observed. Previous studies (33, 34) have proposed acceptable drift values for serviceability and collapse damage states, with 1.9% indicating serviceability loss and 5.0% indicating global column collapse. Based on the obtained results, the maximum drift of all FRC columns remains within the collapse range, indicating an overall improvement in the seismic capacity of the columns.

3. 3. Seismic Fragility The seismic fragility analysis of the structures resulted in the development of fragility curves (FC), which represent the probability of surpassing a specific damage state at a given Intensity Measure (IM). These fragility curves were created using numerical simulations and employed two common methods: the Incremental Dynamic Analysis (IDA) and the cloud approach. The IDA involves incrementally scaling a selected set of earthquake records, while the cloud analysis involves unscaled records. By applying these methods, fragility functions were derived as:

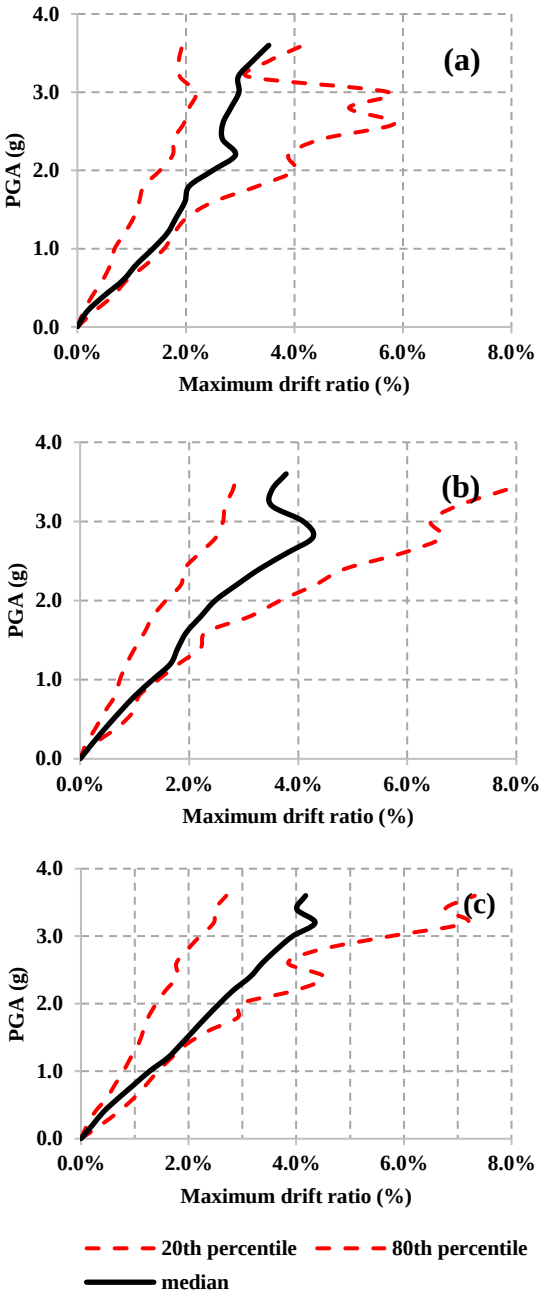

Figure 11. Median and percentiles of IDA curves for maximum drift (%) of different FRC columns: a) PFRC; b) SFRC and c) HyFRC

lognormal cumulative distribution functions (CDF) using Equation 34:

$$P_f(D \geq C|PGA = x) = \Phi(\frac{ln\,(x/c)}{\beta}) \quad (34)$$

In Equation 34, Pf represents the damage probability, PGA is the conditional value of the IM, and D and C denote the column demand and capacity, respectively. The function Φ(.) corresponds to the normal standard

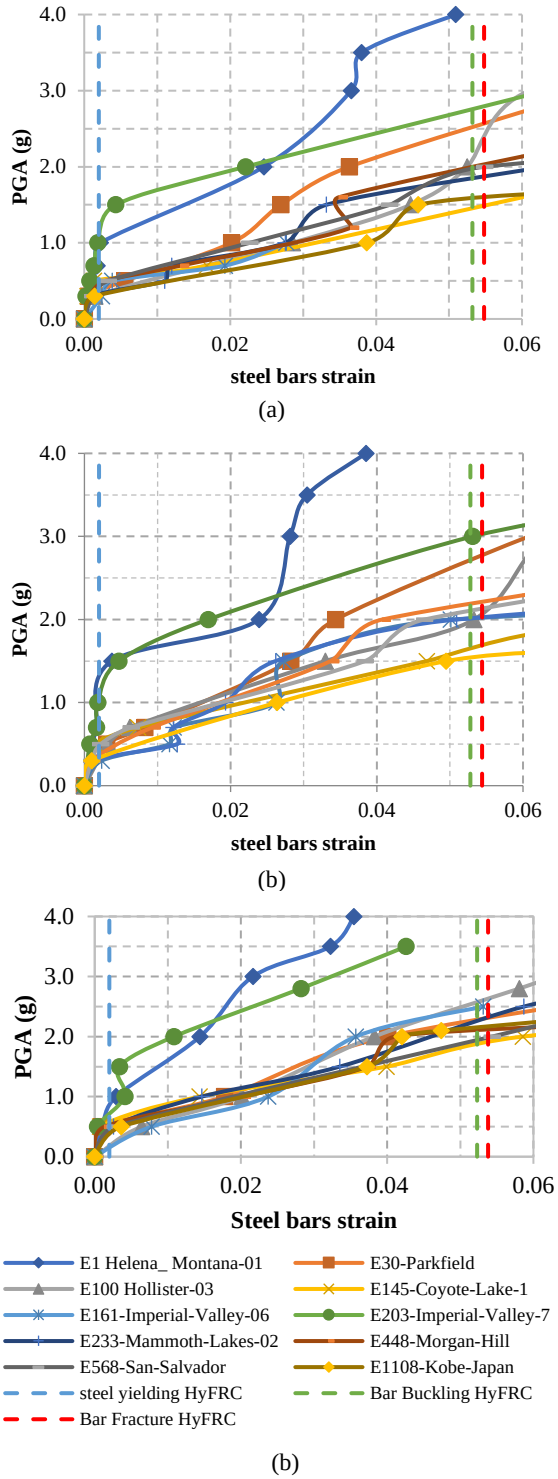

Figure 12. IDA curves for tensile strain of longitudinal reinforcements column with different FRC material: a) SFRC; b) PFRC; and c) HyFRC

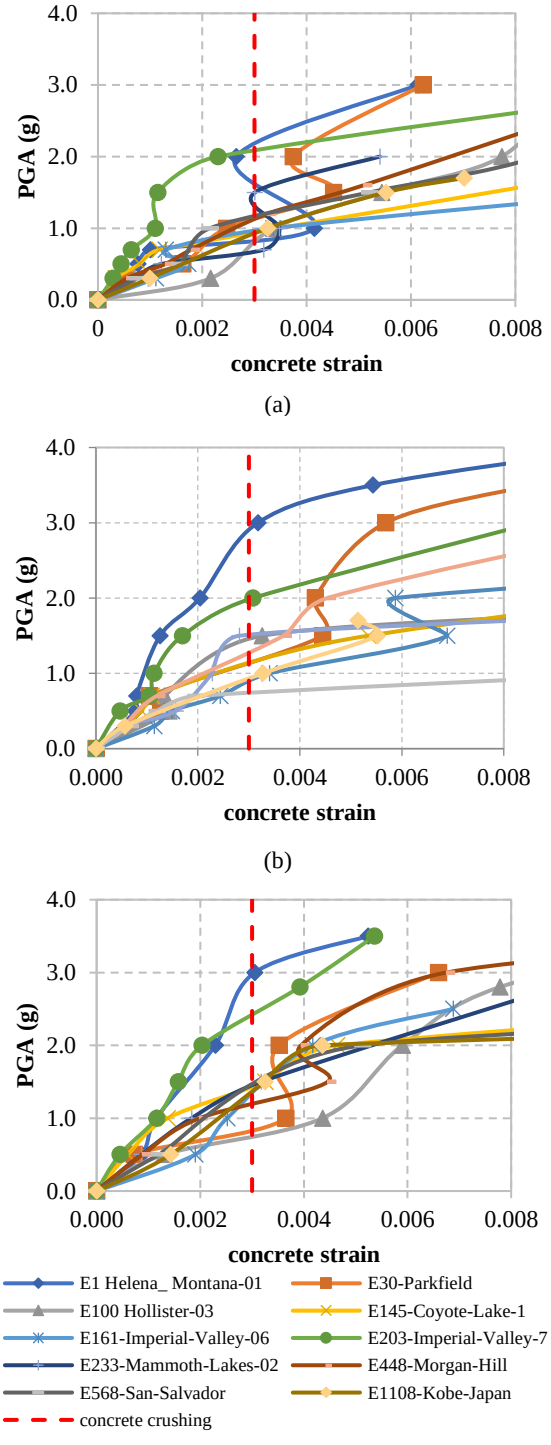

Figure 13. IDA curves for concrete compressive strain of FRC columns material: a) PFRC; b) SFRC; and c) HyFRC

cumulative distribution, while c and β represent the median and standard deviation of the fragility curves, respectively. The estimation of the parameters c and β can be performed using the approach proposed by Baker (35). The damage states considered in this study were defined in section 2. The IDA curves based on the maximum drift ratio were utilized to generate the seismic

fragility curves for the FRC columns at four limit states. Figure 14 illustrates that the HyFRC column exhibits a lower probability of exceeding the damage limit compared to the SFRC and PFRC columns. This indicates that the combination of fibers in RC columns effectively enhances the seismic performance. Moreover, the PFRC and SFRC columns show nearly identical seismic responses for extensive and complete damage states, while the SFRC and HyFRC columns demonstrate a better performance for moderate damage states.

4. RESULTS AND DISCUSSION

4. 1. Nonlinear Static Pushover Analysis The analysis of the pushover curves demonstrates a significant improvement for the FRC column in term of shear capacity compared to RC columns; The HyFRC column exhibit the most significant improvement in seismic capacity, while SFRC and PFRC column ranked second and third. Table 6 illustrates the difference of displacement and base shear at four flexural damage states from the pushover curves. Table 6 provides a detailed breakdown of the disparities in displacement and base shear at four distinct flexural damage states as derived from the pushover curves. For steel yielding damage state, the PFRC is improved by 32 %, the SFRC by 63% and HyFRC by 75%. While for steel bar buckling, the PFRC is improved by 1 %, the SFRC by 17 % and HyFRC by 47 %. For steel bar fracture, the PFRC is improved by 10 %, the SFRC by 27 % and HyFRC by 58 %.

4. 2. Incremental Dynamic Analysis By comparing IDA curves in terms of the maximum drift ratio, it can be concluded that the HyFRC columns experience lower drift ratios than the PFRC and HyFRC columns. Given the design PGA = 1.0 g at high seismic zones, the following maximum drift values are obtained from the fractile IDA curves:

- The 20% IDA curve records maximum drift values of 0.69%, 0.73%, and 0.79% for PFRC, SFRC, and HyFRC, respectively.
- The 50% IDA curve results in maximum drift values of 1.39%, 1.33%, and 1.27% for PFRC, SFRC, and HyFRC, respectively.
- The 80% IDA curve indicates maximum drift values of 1.60%, 1.44%, and 1.43% for PFRC, SFRC, and HyFRC, respectively.

In summary, it is evident that HyFRC is more effective in enhancing seismic capacity and reducing seismic demands compared to SFRC and PFRC.

4. 3. Seismic Fragility Analysis In this study, we consider four predefined damage states: slight, moderate, extensive, and collapse, as previously outlined. Figure 14 presents the seismic fragility curves for the three FRC columns and the four damage states. Overall, there is a clear trend of decreasing damage probability as the damage state becomes more severe. The HyFRC columns are less fragile than the ones where the columns are made of SFRC and PFRC.

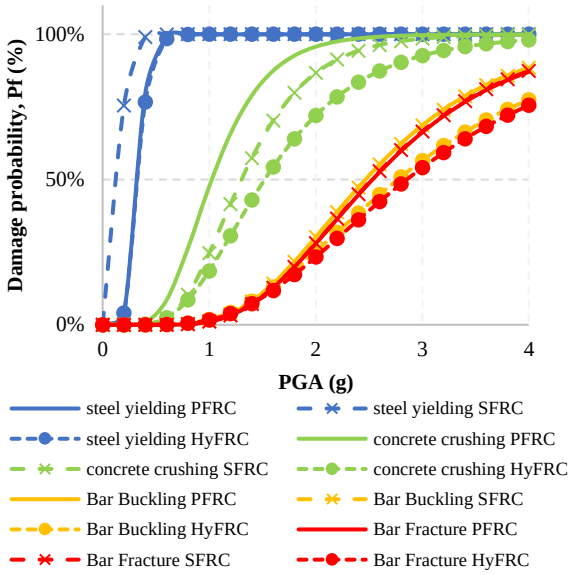

Figure 14. Seismic fragility curves of different FRC columns for four Performance levels

For the slight damage state, both HyFRC and PFRC demonstrate similar vulnerability. For instance, for example, the probability of damage exceedance at 0.2 g PGA is reduced from 75% for SFRC, to 4% for both PFRC and HyFRC.

At the moderate damage state, HyFRC exhibits the lowest damage vulnerability, with the probability of exceedance (for 1.4 g PGA) decreasing to 42.9%, from 57.3% and 78.9% for SFRC and PFRC respectively.

In the extensive damage state, PFRC and SFRC exhibit similar fragility while HyFRC is the least fragile. For a 2.6 g PGA, the probability of exceedance for PFRC and SFRC 44.9%, and 38.4% for HyFRC.

These findings highlight the effectiveness of a hybrid combination of steel and Polypropylene fibers with appropriate proportions in enhancing seismic performance compared to single-type of FRC columns. This is in agreement with previous studies (36, 37).

5. CONCLUSION

This study proposed a combination of CDP and XFEM to investigate the seismic performance of conventional reinforced concrete (RC) and fiber-reinforced concrete (FRC) columns. A 3D finite element model was developed for various FRC columns using appropriate

constitutive laws and the XFEM technique to simulate cracking behavior. The model was calibrated using experimental data.

Nonlinear static pushover analysis (NSPA) was employed to evaluate the flexural damage states, and incremental dynamic analysis (IDA) was conducted on all FRC columns using a suite of 10 near-fault earthquake records. The maximum drift was selected as the engineering demand parameter (EDP) to compare the seismic behavior of different FRC columns. Based on the NSPA and IDA analysis results, the following conclusions can be drawn:

1. From the Pushover curves, it can be seen that there is a significant improvement for the FRC column in term of shear capacity compared to RC columns for all damage states.
2. By comparing IDA curves in terms of the maximum drift ratio, it can be concluded that the HyFRC columns experience lower drift ratios than the PFRC and HyFRC columns. Thus, it can be concluded that HyFRC are more effective to improve the seismic capacity and reduce the seismic demands of the column, compared to SFRC and PFRC.
3. The Seismic fragility analysis was conducted on the three FRC columns and the four damage states. The HyFRC columns are less fragile than the ones where the columns are made of SFRC and PFRC. Which highlights the effectiveness of a hybrid combination of steel and Polypropylene fibers in enhancing seismic performance compared to single-type of FRC columns.

6. REFERENCES

1. Mohammed AH, Mubarak HM, Hussein AK, Abulghafour TZ, Nassani DE. Punching Shear Characterization of Steel Fiber-Reinforced Concrete Flat Slabs. HighTech and Innovation Journal. 2022;3(4):483-90.
2. Bouzid L, Hamizi M, Hannachi N-E, Nekmouche A, Akkouche K. Plastic hinges mechano-reliability analysis in the beams of RC frames structures. World Journal of Engineering. 2020;17(5):719-32. 10.1108/WJE-02-2020-0069
3. Fanning PJ, Boothby TE. Three-dimensional modelling and full-scale testing of stone arch bridges. Computers & Structures. 2001;79(29-30):2645-62. 10.1016/S0045-7949(01)00109-2
4. Brencich A, Sabia D. Experimental identification of a multi-span masonry bridge: The Tanaro Bridge. Construction and Building Materials. 2008;22(10):2087-99. 10.1016/J.CONBUILDMAT.2007.07.031
5. Reccia E, Milani G, Cecchi A, Tralli A. Full 3D homogenization approach to investigate the behavior of masonry arch bridges: The Venice trans-lagoon railway bridge. Construction and Building Materials. 2014;66:567-86. 10.1016/J.CONBUILDMAT.2014.05.096
6. LI S, Yu T, Jia J. Empirical seismic vulnerability and damage of bottom frame seismic wall masonry structure: A case study in Dujiangyan (China) region. International Journal of Engineering, Transactions C: Aspects. 2019;32(9):1260-8. 10.5829/ije.2019.32.09c.05
7. Xiong Z, Chen J, Liu C, Li J, Li W. Bridge's Overall Structural Scheme Analysis in High Seismic Risk Permafrost Regions. Civil Engineering Journal. 2022;8(7):1316-27. 10.28991/CEJ-2022-08-07-01
8. Kamrani Moghaddam P, Manafpour A. Effects of Far-and Near-Field Multiple Earthquakes on the RC SDOF Fragility Curves Using Different First Shock Scaling Methods. International Journal of Engineering, Transactions C: Aspects,. 2018;31(9):1505-13. 10.5829/ije.2018.31.09c.05
9. Conde B, Ramos LF, Oliveira DV, Riveiro B, Solla M. Structural assessment of masonry arch bridges by combination of non-destructive testing techniques and three-dimensional numerical modelling: Application to Vilanova bridge. Engineering Structures. 2017;148:621-38. 10.1016/J.ENGSTRUCT.2017.07.011
10. Cannizzaro F, Pantò B, Caddemi S, Caliò I. A Discrete Macro-Element Method (DMEM) for the nonlinear structural assessment of masonry arches. Engineering Structures. 2018;168:243-56. 10.1016/J.ENGSTRUCT.2018.04.006
11. Milani G, Lourenço PB. 3D non-linear behavior of masonry arch bridges. Computers & Structures. 2012;110:133-50. 10.1016/J.COMPSTRUC.2012.07.008
12. Oliveira DV, Lourenço PB, Lemos C. Geometric issues and ultimate load capacity of masonry arch bridges from the northwest Iberian Peninsula. Engineering Structures. 2010;32(12):3955-65. 10.1016/J.ENGSTRUCT.2010.09.006
13. Asadi P, Sourani H. Fragility curves production by seismic improvement of the high-dimensional model representation method. Engineering Computations. 2020;37(1):120-43. 10.1108/EC-12-2018-0586
14. Zhang Y, Macorini L, Izzuddin BA. Numerical investigation of arches in brick-masonry bridges. Structure and Infrastructure Engineering. 2018;14(1):14-32. 10.1080/15732479.2017.1324883
15. Baharmast H, Razmyan S, Yazdani A. Approximate incremental dynamic analysis using reduction of ground motion records. International Journal of Engineering, Transactions B: Applications. 2015;28(2):190-7. 10.5829/idosi.ije.2015.28.02b.04
16. Luco N, Cornell CA, editors. Effects of random connection fractures on the demands and reliability for a 3-story pre-Northridge SMRF structure. Proceedings of the 6th US national conference on earthquake engineering; 1998: Citeseer.
17. Vamvatsikos D, Cornell CA. Incremental dynamic analysis. Earthquake engineering & structural dynamics. 2002;31(3):491-514. 10.1002/eqe.141
18. Mohamed Nazri F, Kian Yern C, Moffed Kassem M, Noroozinejad Farsangi E. Assessment of structure-specific fragility curves for soft storey buildings implementing IDA and SPO approaches. International Journal of Engineering, Transactions C: Aspects,. 2018;31(12):2016-21. 10.5829/ije.2018.31.12c.04
19. Singh V, Sangle K. Analysis of vertically oriented coupled shear wall interconnected with coupling beams. HighTech and Innovation Journal. 2022;3(2):230-42. 10.28991/HIJ-2022-03-02-010
20. Zhang Y, Dias-da-Costa D. Seismic vulnerability of multi-span continuous girder bridges with steel fibre reinforced concrete columns. Engineering Structures. 2017;150:451-64. 10.1016/j.engstruct.2017.07.053
21. Huang L, Xu L, Chi Y, Xu H. Experimental investigation on the seismic performance of steel–polypropylene hybrid fiber reinforced concrete columns. Construction and Building Materials. 2015;87:16-27. 10.1016/j.conbuildmat.2015.03.073

22. Chi Y, Xu L, Zhang Y. Experimental study on hybrid fiber–reinforced concrete subjected to uniaxial compression. Journal of Materials in Civil Engineering. 2014;26(2):211-8. 10.1061/(ASCE)MT.1943-5533.0000764
23. Lubliner J, Oliver J, Oller S, Onate E. A plastic-damage model for concrete. International Journal of solids and structures. 1989;25(3):299-326. 10.1016/0020-7683(89)90050-4
24. Lee J, Fenves GL. Plastic-damage model for cyclic loading of concrete structures. Journal of engineering mechanics. 1998;124(8):892-900. 10.1061/(asce)0733-9399(1998)124:8(892)
25. Chi Y, Yu M, Huang L, Xu L. Finite element modeling of steel-polypropylene hybrid fiber reinforced concrete using modified concrete damaged plasticity. Engineering Structures. 2017;148:23-35. 10.1016/j.engstruct.2017.06.039
26. Abadel A, Abbas H, Almusallam T, Al-Salloum Y, Siddiqui N. Mechanical properties of hybrid fibre-reinforced concrete–analytical modelling and experimental behaviour. Magazine of Concrete Research. 2016;68(16):823-43. 10.1680/jmacr.15.00276
27. Hordijk D. Local Approach to Fatigue of Concrete Delft University of Technology. 1991.
28. Almusallam T, Ibrahim S, Al-Salloum Y, Abadel A, Abbas H. Analytical and experimental investigations on the fracture behavior of hybrid fiber reinforced concrete. Cement and Concrete Composites. 2016;74:201-17. 10.1016/j.cemconcomp.2016.10.002
29. Rousakis TC, Karabinis AI, Kiousis PD, Tepfers R. Analytical modelling of plastic behaviour of uniformly FRP confined concrete members. Composites Part B: Engineering. 2008;39(7-8):1104-13. 10.1016/J.COMPOSITESB.2008.05.001
30. Liang X, Xing P, Xu J. Experimental and numerical investigations of the seismic performance of columns with fiber-reinforced concrete in theplastic hinge region. Advances in Structural Engineering. 2016;19(9):1484-99. 10.1177/1369433216643896
31. Paulay T, Priestley MN. Seismic design of reinforced concrete and masonry buildings: Wiley New York; 1992.
32. Berry MP, Eberhard MO. Performance modeling strategies for modern reinforced concrete bridge. University of California, Berkeley. 2008.
33. Kowalsky MJ. Deformation limit states for circular reinforced concrete bridge columns. Journal of Structural Engineering. 2000;126(8):869-78. 10.1061/(ASCE)0733-9445(2000)126:8(869)
34. Liu M, Lu B, Liu B, editors. Study on performance index of reinforced concrete bridge column. Software Engineering and Knowledge Engineering: Theory and Practice: Volume 1; 2012: Springer. 10.4028/www.scientific.net/AMM.193-194.1079
35. Baker JW. Efficient analytical fragility function fitting using dynamic structural analysis. Earthquake Spectra. 2015;31(1):579-99. 10.1193/021113EQS025M
36. Pang Y, Cai L, Ouyang H, Zhou X. Seismic performance assessment of different fibers reinforced concrete columns using incremental dynamic analysis. Construction and Building Materials. 2019;203:241-57. 10.1016/j.cscm.2023.e02303
37. Zhang C, Cao M. Fiber synergy in multi-scale fiber-reinforced cementitious composites. Journal of Reinforced Plastics and Composites. 2014;33(9):862-74. 10.1177/0731684413514785

Persian Abstract

چکیده

اطمینان از مقاومت لرزه ای در مناطق زلزله خیز برای ایمنی سازه ضروری است. ستون های بتن تقویت شده با الیاف (FRC) نویدبخش بهبود عملکرد سازه در شرایط لرزه ای هستند. این مطالعه به دنبال ارزیابی جامع رفتار لرزه ای آنهاست. هدف اصلی این تحقیق ارزیابی و مقایسه عملکرد لرزه ای انواع ستون های FRC از جمله الیاف پلی پروپیلن (PFRC)، الیاف فولادی (SFRC) و ترکیبات ترکیبی (HyFRC) در مقایسه با ستون های بتن مسلح معمولی (RC) است. برای دستیابی به این هدف، این مطالعه از روش المان محدود توسعه‌یافته همراه با پلاستیسیته آسیب بتن (XFEM-CDP) در آباکوس برای بررسی دقیق پاسخ‌های استاتیکی و دینامیکی استفاده می‌کند. تجزیه و تحلیل فشار اور استاتیکی غیرخطی بهبود قابل توجهی در مقاومت لرزه ای در تمام انواع FRC در مقایسه با ستون های RC نشان داد. تحلیل‌های دینامیکی افزایشی (IDA) با استفاده از مجموعه انتخابی از ۱۰ حرکت زمین نزدیک به گسل برای ارزیابی پاسخ‌های لرزه‌ای غیرالاستیک ستون‌های پل FRC مختلف انجام می‌شود. شبیه‌سازی‌های XFEM-CDP در Abaqus جنبه‌های متعددی از ستون‌های FRC، مانند ترک‌خوردگی بتن، کاهش سختی و رفتار پلاستیک را به تصویر می‌کشند. تجزیه و تحلیل شکنندگی لرزه ای این ستون های FRC با در نظر گرفتن چهار حالت آسیب انجام می شود: الف) تسلیم طولی فولاد، ب) خرد شدن بتن هسته، ج) کمانش میله فولادی، و د) شکستگی میله فولادی طولی. نتایج نشان داد که ستون های HyFRC کمترین آسیب پذیری آسیب را در مقایسه با انواع PFRC و SFRC نشان می دهند.